



Deposited via The University of Leeds.

White Rose Research Online URL for this paper:

<https://eprints.whiterose.ac.uk/id/eprint/193992/>

Version: Accepted Version

---

**Proceedings Paper:**

Nie, L, Toulemonde, M, Tang, M-X et al. (2022) 3D Localization of Scatterers with a Spiral-Shaped Acoustic Lens. In: 2022 IEEE International Ultrasonics Symposium (IUS). 2022 IEEE International Ultrasonics Symposium (IUS), 10-13 Oct 2022, Venice, Italy. IEEE. ISBN: 978-1-6654-7813-7. ISSN: 1948-5719. EISSN: 1948-5727.

<https://doi.org/10.1109/IUS54386.2022.9958492>

---

© 2022 IEEE. Personal use of this material is permitted. Permission from IEEE must be obtained for all other uses, in any current or future media, including reprinting/republishing this material for advertising or promotional purposes, creating new collective works, for resale or redistribution to servers or lists, or reuse of any copyrighted component of this work in other works.

**Reuse**

Items deposited in White Rose Research Online are protected by copyright, with all rights reserved unless indicated otherwise. They may be downloaded and/or printed for private study, or other acts as permitted by national copyright laws. The publisher or other rights holders may allow further reproduction and re-use of the full text version. This is indicated by the licence information on the White Rose Research Online record for the item.

**Takedown**

If you consider content in White Rose Research Online to be in breach of UK law, please notify us by emailing [eprints@whiterose.ac.uk](mailto:eprints@whiterose.ac.uk) including the URL of the record and the reason for the withdrawal request.

# 3D Localization of Scatterers with a Spiral-Shaped Acoustic Lens

Luzhen Nie<sup>1</sup>, Matthieu Toulemonde<sup>2</sup>, Meng-Xing Tang<sup>2</sup>, Steven Freear<sup>1</sup>, and Sevan Harput<sup>3</sup>

<sup>1</sup>School of Electronic and Electrical Engineering, University of Leeds, Leeds, U.K.

<sup>2</sup>Department of Bioengineering, Imperial College London, London, U.K.

<sup>3</sup>Division of Electrical and Electronic Engineering, London South Bank University, London, U.K.

E-mail: harputs@lsbu.ac.uk

**Abstract**— Traditionally, single element transducers are used for localizing objects in 1D through A-mode scans, where only the echo envelope is used. Due to the transducer surface symmetry, A-mode scans performed for azimuthally or elevationally translated scatterers will produce the same 1D information, radial distance. The current study extends the previous work to investigate scatterer localization in 3D by breaking this surface symmetry with the attachment of a new acoustic lens to a single element transducer.

In this work, an acoustic lens was 3D printed with a spiral-shaped pattern to partially block the ultrasound waves. When the ultrasound waves are blocked in an anisotropic manner, the symmetry of the transducer is broken. Therefore, the acoustic lens acts as a spatial filter and encodes the received echoes unambiguously, where it is possible to decode the received signals and extract directional information. With this technology, a single sensor can acquire multi-dimensional information with a single measurement.

**Keywords**—Acoustic lens, Single element imaging, 3D imaging, 3D localization

## I. INTRODUCTION

Complexity of ultrasound systems increase significantly while transitioning from 2D to 3D imaging, since a larger number of elements and active channels are required. Various methods have been proposed to reduce complexity of ultrasound systems for 3D imaging by decreasing the number of imaging channels, such as element multiplexing [1, 2], row-column addressing [3, 4], sparse arrays [5-10], mechanical rotation or translation of 1-D ultrasound arrays [11, 12] and imaging through a rotating lens attached to a single ultrasound transducer [13-16].

Single element transducer are often used to perform an A-mode scan, which is used to detect the depth of a reflector or scatterer. In this case, only the envelope of the received signal is used to estimate the axial distance (or the radial distance,  $r$ ) of a scatterer. When the phase of the signal is used, as explained in [17], scatterers can be localized in 2D,  $(r, \theta)$ .

In this work, a new approach is proposed to address the 3D localization problem using a single element transducer. An acoustic lens with an embedded spiral-shaped pattern was designed to enhance the detection capacity of single element ultrasound transducers. The proposed acoustic lens design was verified by a simulation study and an experimental demonstration was performed using a 3D printed acoustic lens. Results showed that it can be possible to detect the location of a

scatter using the proposed technology in multiple spatial dimensions (elevation, azimuth and axial), if the number of scatterers in the ultrasonic field is sparse.

## II. PROBLEM STATEMENT

Figure 1 shows three different scatterers located at the same distance from the transducer with different polar and azimuthal angles. When the A-mode method is used, echoes received from these three scatterers will result in the same radial distance estimation through a time-of-flight measurement based on the envelope of the received signal. Although the envelopes of the received signals are almost identical, the phase and frequency of the received signals through the acoustic lens will be different, which can be found in the results section.

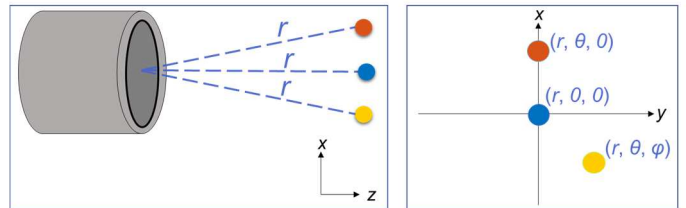


Fig. 1. Schematic of three different scenarios used to highlight the importance of breaking the transducer surface symmetry. (Left)  $x$ - $z$  view of the scatterers. (Right)  $x$ - $y$  view of the scatterers.

## III. METHODS

### A. Simulations

The initial verification was performed using the Field II simulation toolbox in Matlab [18, 19]. A single element transducer of 6-mm diameter working at 2.4 MHz was chosen for simulations to align with the working frequency of the transducer used in experiments. For the numerical verification, received signals from the single element transducer with and without a spiral-shaped mask, shown in Figure 2, was compared.

Two sets of simulations were performed to test the functionality of the acoustic lens. In the first set of measurements, a point scatterer was placed at three locations  $(r=40 \text{ mm}, \theta=0^\circ, \varphi=0^\circ)$ ,  $(r=40 \text{ mm}, \theta=4.5^\circ, \varphi=0^\circ)$  and  $(r=40 \text{ mm}, \theta=4.5^\circ, \varphi=135^\circ)$  to replicate the problem described in Figure 1. In the second set of simulations, a point scatterer was moved to different locations to verify that the frequency and phase information change unambiguously when the spiral-shaped mask is placed in front of the single-element transducer.

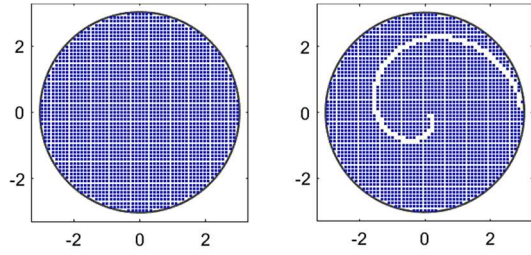


Fig. 2. Active aperture of the transducers used in the simulations. Small blue squares represent the active sub-elements of the transducer on the simulation grid. (Left) Single element transducer without a mask, which is used as a control. (Right) Single element transducer with a spiral shaped mask.

### B. Experiments

A human-pinna-shape-inspired lens with a spiral mask was 3D printed by using an ABS-like resin with a thickness of 0.6 mm and a diameter of 9.6 mm. The lens had a spiral-shaped groove (air channels) on one side to create the surface asymmetry by locally blocking the arriving ultrasound waves as shown in Figure 3.

The experimental setup consisted of a single element transducer, an acoustic lens and the Ultrasound Array Research Platform (UARP) [20, 21]. The UARP was connected to a 6 mm diameter single-element transducer (V323-SM, Olympus IMS, MA) to transmit and receive the ultrasound signals. The single-element transducer was driven with a one-cycle sinusoidal signal at 2.4 MHz center frequency. A sub-wavelength target (a 200  $\mu\text{m}$  wire) placed in water was used in the experimental measurements. For each measurement, the target was moved to a different location using a translation stage to replicate the conditions of the second set of simulation.



Fig. 3. (Left) 3D drawing of the acoustic lens with a spiral-shaped mask. (Right) Photograph of the transducer with the attached acoustic lens.

## IV. RESULTS AND DISCUSSION

### A. First set of simulations

To reproduce the initial problem described in Figure 1, the first set of simulations are performed with three point scatterers located at the following spherical  $(r, \theta, \phi)$  coordinates:  $(40 \text{ mm}, 0^\circ, 0^\circ)$ ,  $(40 \text{ mm}, 4.5^\circ, 0^\circ)$  and  $(40 \text{ mm}, 4.5^\circ, 135^\circ)$ . Without the lens, equidistant scatterers cannot be differentiated using A-mode envelopes, as shown in Figure 4 (Top). The measurements without a spiral-shaped mask are provided as a control, where the received signals from scatterers with an angle of  $\theta=4.5^\circ$  are almost identical and cannot be used to localize scatterers in 3D.

However, when the surface symmetry is broken by a defect embedded within the lens, ultrasound waves arriving from different directions are distorted in a distinct manner. As shown in Figure 4 (Bottom), the effect of the asymmetric spatial response is significant, so the change of the scatterer location (even for equidistant locations to the transducer axis) results in the alteration of temporal waveforms and spectra. The radial depth can be determined based on the time of flight using the envelope peak of the time domain signal, similar to an A-mode

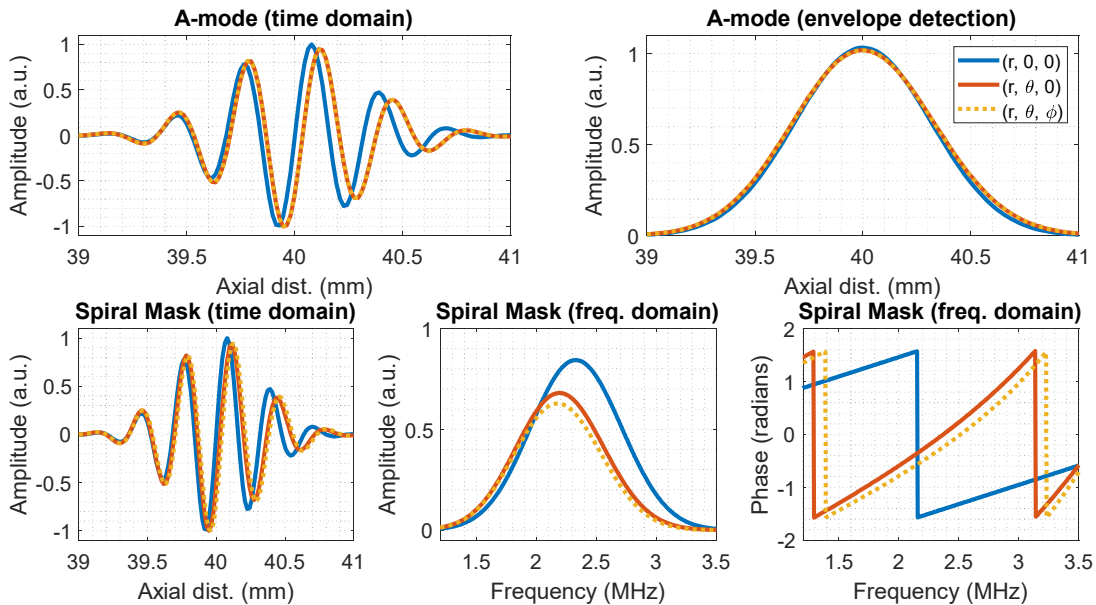


Fig. 4. Comparisons between A-mode and the proposed method using an acoustic lens with a spiral-shaped mask. Both methods are compared for the three scenarios illustrated in Figure 1. (Top) Received signals without a lens, A-mode envelope peaks appear at the same location and it is not possible to differentiate the scatterer locations. (Bottom) Received signals for the transducer with the spiral-shaped mask is shown in time and frequency domains. There are noticeable changes in the frequency peak and the phase of the received signal which can be used to find the location of a scatterer in 3D.

scan, which is at 40 mm. The elevational angle can be estimated by the shift of the frequency peak, where the frequency peak is at 2.33 MHz for the scatterer located at (40 mm,  $0^\circ$ ,  $0^\circ$ ) and the peak is at 2.19 MHz for the other two scatterers located with an angle of  $\theta=4.5^\circ$ . The zero-crossing point of the spectral phase can be used to localize the azimuthal angle of scatterers, where the zero-crossing is at 2.37 MHz for  $\varphi = 0^\circ$  and 2.54 MHz for  $\varphi = 135^\circ$ . By employing these changes in the frequency response of the received signals, the proposed method could enable the 3D localization capability of single element transducers with a single acquisition.

### B. Second set of simulations and experimental demonstration

For this set of simulations and experiments, seven different scatterers are located at the following spherical ( $r$ ,  $\theta$ ,  $\varphi$ ) coordinates;  $r = 40$  mm and  $\varphi = 0^\circ$  with a varying polar angle of  $\theta = 0.72^\circ$ ,  $1.43^\circ$ ,  $2.15^\circ$ ,  $2.87^\circ$ ,  $3.58^\circ$  and  $4.3^\circ$  in spherical coordinates. These locations correspond to the lateral translation of a scatterer in x-direction as  $x = 0, 0.5, 1.0, 1.5, 2.0, 2.5$  and  $3.0$  mm.

Figure 5 shows the received signals in the time domain and their corresponding spectra and phase responses acquired using an acoustic lens with a spiral-shaped mask. For measurements at different lateral positions, the echo amplitude changes according to the beam profile shown in Figure 5 (Left) as expected, since the off-axis scatterers result in a weaker echo. The magnitude of the frequency response given in Figure 5 (Middle) shows that the received echoes are filtered by the transducer's spatial response, which changes with the elevational angle of incidence,  $\theta$ . This spatial filtering effect is so significant that small changes in the lateral position of the scatterer alters the received signal and causes a shift in the spectral peak. Figure 5 (Right) shows the phase response of each measurement. Although the phase response of the experimentally acquired signals are significantly different from the simulated signals, the point to highlight is that they all have different zero-crossings and can be used for 3D localization of scatterers.

There are some differences between the simulated and experimentally acquired waveforms, shown in Figure 5, due to the following reasons. When the 3D printed acoustic lens is placed in front of the transducer, reverberations occur inside the acoustic lens, so the received time domain waveforms have tails. In the simulations, the acoustic lens is implemented with zero thickness (an ideal lens for this work), which does not create such secondary reflections. The other discrepancy between the simulations and the experiments is the temporal shift of the received signals. In the experiments, the transducer is only moved along the x-direction with a distance up to 3 mm at increments of 0.5 mm, where the radial distance effectively changes between 40 and 40.22 mm for these experimental measurements due to the limitation of the translation stage.

## V. CONCLUSIONS

The spiral-shaped acoustic lens technology could extend the localization capabilities of single-element ultrasonic transducers by encoding the phase and frequency content of the received signal from a single channel. Therefore, this technology can be used to find the location of a single smaller-than-wavelength scatterer by using only a single measurement.

Each ultrasound transducer and the acoustic lens require a set of calibration measurements to model the phase and the frequency response of the system. After the calibration process, the proposed technology can be used without a requirement of high complexity ultrasound hardware or mechanical movement, as the extraction of the directional information is performed in software.

## ACKNOWLEDGMENT

The authors would like to acknowledge the support from the Royal Society under grant RGS\R1\201012 and U.K. EPSRC under grant EP/P023266/1.

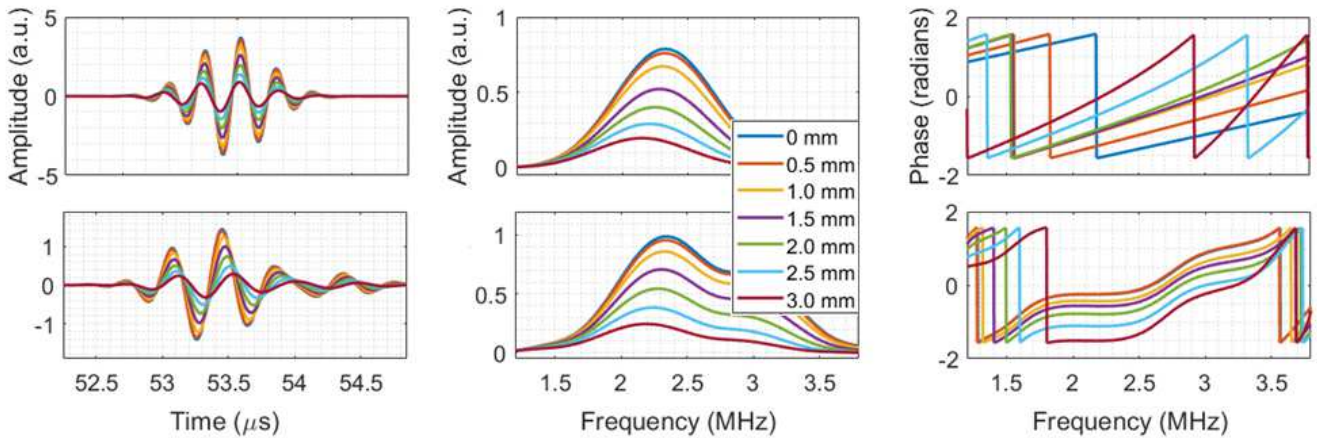


Fig. 5. (Top) Simulations and (Bottom) experimental measurements performed using the acoustic lens with a spiral-shaped mask shown in Figures 2 and 3, respectively. Received echoes from scatterers located at varying lateral locations are shown (Left) in the time domain with corresponding (Middle) spectral magnitude and (Right) phase responses. Scatterers are located with a distance between 0 and 3.0 mm in a lateral direction and 40 mm away from the transducer in depth.

## REFERENCES

- [1] J. Provost, C. Papadacci, J. E. Arango, M. Imbault, M. Fink, J.-L. Gennisson, M. Tanter, and M. Pernot, "3-d ultrafast ultrasound imaging in vivo," *Physics in Medicine & Biology*, vol. 59, no. 19, p. L1, 2014.
- [2] J.-l. Gennisson, J. Provost, T. Deffieux, C. Papadacci, M. Imbault, M. Pernot, and M. Tanter, "4-d ultrafast shear-wave imaging," *IEEE Trans. Ultrason., Ferroelectr., Freq. Control*, vol. 62, no. 6, pp. 1059–1065, 2015.
- [3] M. F. Rasmussen, T. L. Christiansen, E. V. Thomsen, and J. A. Jensen, "3-d imaging using row-column-addressed arrays with integrated apodization - part i: Apodization design and line element beamforming," *IEEE Trans. Ultrason., Ferroelectr., Freq. Control*, vol. 62, no. 5, pp. 947–958, 2015.
- [4] M. Flesch, M. Pernot, J. Provost, G. Ferin, A. Nguyen-Dinh, M. Tanter, and T. Deffieux, "4-d in vivo ultrafast ultrasound imaging using a row-column addressed matrix and coherently-compounded orthogonal plane waves," *Physics in Medicine & Biology*, vol. 62, no. 11, p. 4571, 2017.
- [5] A. Austeng and S. Holm, "Sparse 2-d arrays for 3-d phased array imaging-design methods," *IEEE Trans. Ultrason., Ferroelectr., Freq. Control*, vol. 49, no. 8, pp. 1073–1086, 2002.
- [6] B. Diarra, M. Robini, P. Tortoli, C. Cachard, and H. Liebgott, "Design of optimal 2-d non-grid sparse arrays for medical ultrasound," *IEEE Transactions on Biomedical Engineering*, vol. 60, no. 11, pp. 3093–3102, 2013.
- [7] A. Ramalli, E. Boni, A. S. Savoia, and P. Tortoli, "Density-tapered spiral arrays for ultrasound 3-d imaging," *IEEE Trans. Ultrason., Ferroelectr., Freq. Control*, vol. 62, no. 8, pp. 1580–1588, 2015.
- [8] E. Roux, A. Ramalli, P. Tortoli, C. Cachard, M. C. Robini, and H. Liebgott, "2-d ultrasound sparse arrays multi-depth radiation optimization using simulated annealing and spiral-array inspired energy functions," *IEEE Trans. Ultrason., Ferroelectr., Freq. Control*, vol. 63, no. 12, pp. 2138–2149, 2016.
- [9] S. Harput, K. Christensen-Jeffries, A. Ramalli, J. Brown, J. Zhu, G. Zhang, C. H. Leow, M. Toulemonde, E. Boni, P. Tortoli et al., "3-d super-resolution ultrasound imaging with a 2-d sparse array," *IEEE Trans. Ultrason., Ferroelectr., Freq. Control*, vol. 67, no. 2, pp. 269–277, 2019.
- [10] S. Harput, K. Christensen-Jeffries, J. Brown, J. Zhu, G. Zhang, C. H. Leow, M. Toulemonde, A. Ramalli, E. Boni, P. Tortoli et al., "3-d super-resolution ultrasound imaging using a 2-d sparse array with high volumetric imaging rate," in *IEEE International Ultrasonics Symposium (IUS)*, 2018, pp. 1–4.
- [11] G. M. Treece, A. H. Gee, R. W. Prager, C. J. Cash, and L. H. Berman, "High-definition freehand 3-d ultrasound," *Ultrasound in Medicine & Biology*, vol. 29, no. 4, pp. 529–546, 2003.
- [12] J. Zhu, E. M. Rowland, S. Harput, K. Riemer, C. H. Leow, B. Clark, K. Cox, A. Lim, K. Christensen-Jeffries, G. Zhang et al., "3-d super-resolution us imaging of rabbit lymph node vasculature in vivo by using microbubbles," *Radiology*, vol. 291, no. 3, pp. 642–650, 2019.
- [13] P. Kruizinga, P. van der Meulen, A. Fedjajevs, F. Mastik, G. Springeling, N. de Jong, J. G. Bosch, and G. Leus, "Compressive 3-d ultrasound imaging using a single sensor," *Science Advances*, vol. 3, no. 12, pp. e1701423, 2017.
- [14] P. van der Meulen, P. Kruizinga, J. G. Bosch, and G. Leus, "Coding mask design for single sensor ultrasound imaging," *IEEE Transactions on Computational Imaging*, vol. 6, pp. 358–373, 2019.
- [15] J. Janjic, P. Kruizinga, P. Van Der Meulen, G. Springeling, F. Mastik, G. Leus, J. G. Bosch, A. F. van der Steen, and G. van Soest, "Structured ultrasound microscopy," *Applied Physics Letters*, vol. 112, no. 25, pp. 251901, 2018.
- [16] P. van der Meulen, P. Kruizinga, J. G. Bosch, and G. Leus, "Joint optimization of coding mask and scan positions for compressive single sensor imaging," in *IEEE International Ultrasonics Symposium (IUS)*, 2018, pp. 1–4.
- [17] L. Nie, J. T. M. Moo, M. Toulemonde, M-X. Tang, S. Freear, and S. Harput, "Localization of a Scatterer in 3D with a Single Measurement and Single Element Transducer", in *IEEE International Ultrasonics Symposium (IUS)*, 2020, pp. 1-4.
- [18] J. A. Jensen, "Field: A program for simulating ultrasound systems", *10th Nordicbaltic Conference On Biomedical Imaging*, vol. 4, no. 1, pp. 351-353, 1996.
- [19] J. A. Jensen and N. B. Svendsen, "Calculation of pressure fields from arbitrarily shaped apodized and excited ultrasound transducers", *IEEE Trans. Ultrason., Ferroelectr., Freq. Control*, vol. 39, no. 2, pp. 262-267, 1992.
- [20] P. R. Smith, D. M. J. Cowell, B. Raiton, C. V. Ky, and S. Freear, "Ultrasound array transmitter architecture with high timing resolution using embedded phase-locked loops," *IEEE Trans. Ultrason., Ferroelectr., Freq. Control*, vol. 59, no. 1, pp. 40–49, 2012.
- [21] D. M. J. Cowell, P. R. Smith, and S. Freear, "Phase-inversion-based selective harmonic elimination (PI-SHE) in multi-level switched-mode tone- and frequency- modulated excitation," *IEEE Trans. Ultrason., Ferroelectr., Freq. Control*, vol. 60, no. 6, pp. 1084–1097, 2013.